

Thermoelectric Properties of Spark Plasma-Sintered In₄Se₃-In₄Te₃

JA YOUNG CHO,^{1,2} YOUNG SOO LIM,^{1,3} SOON-MOK CHOI,¹
KYOUNG HUN KIM,¹ WON-SEON SEO,¹ and HYUNG-HO PARK²

1.—Korea Institute of Ceramic Engineering and Technology, 233-5 Gasan-dong, Geumcheon-gu, Seoul 153-801, Korea. 2.—Department of Materials Science and Engineering, Yonsei University, 134 Sinchon-dong, Seodaemun-gu, Seoul 120-749, Korea. 3.—e-mail: yslim@kicet.re.kr

We report the thermoelectric properties of spark plasma-sintered In₄Se₃-In₄Te₃ materials. For comparison, pure In₄Se₃ and In₄Se₃ (80 wt.%)/In₄Te₃ (20 wt.%) mixture samples were prepared. In₄Se₃ and In₄Te₃ powders were synthesized by a conventional melting process in evacuated quartz ampoules, and a spark plasma method was used for the sintering of the pure In₄Se₃ and mixture samples. Thermoelectric and structural characterizations were carried out, and the mixing effect of In₄Se₃ and In₄Te₃ on the thermoelectric properties was investigated.

Key words: In₄Se₃, In₄Te₃, mixture, thermoelectric, figure of merit

INTRODUCTION

In₄Se₃ consisting of quasi-two-dimensional covalent bond layers and quasi-one-dimensional In chains has received considerable attention because of its superb thermoelectric performance.¹⁻³ The performance of a thermoelectric material can be quantified by the dimensionless figure of merit, $ZT = S^2\sigma T/\kappa$, where S , σ , T , and κ are the Seebeck coefficient, electrical conductivity, absolute temperature, and thermal conductivity, respectively. The electrical conductivity (σ) of In₄Se₃ with a small direct band gap of 0.2 eV can be controlled by Se-deficient self-doping.² A high negative Seebeck coefficient (S) of up to $-500 \mu\text{V/K}$ has been reported, and it is also affected by the self-doping conditions.²

Thermal conductivity is a very important factor to obtain high thermoelectric performance.^{4,5} It has been reported that very low thermal conductivity (κ) can be obtained due to the unique features of the low-dimensional structure of In₄Se₃. Peierls distortion by a charge density wave leads to breakage in the translational symmetry, and a condensate state due to strong electron-phonon interactions induces

structural defects in the In₄Se₃ lattice.^{1,6,7} These defects can restrain the thermal conduction by phonon scattering. Moreover, the abundance of low-frequency phonon modes in In₄Se₃ also influences the thermal conductivity.^{8,9} Consequently, In₄Se₃ can possess a very low thermal conductivity of less than 1.0 W/mK.¹⁻³

Interestingly, the space group of In₄Te₃ is $D2h^{12}-P_{nnm}$, the same as that of In₄Se₃.¹⁰ Therefore, as in In₄Se₃, a low thermal conductivity due to the low-dimensional structure can be expected in In₄Te₃. Moreover, the large mass of the tellurium atoms can impact the thermal conductivity of this class of layered thermoelectric material.¹⁰ Also, the same valences of Se and Te and the similar lattice parameters of In₄Te₃ and In₄Se₃ may provide the possibility of discovering a new composition in the In₄Se₃-In₄Te₃ thermoelectric material system.

Herein, we report the thermoelectric properties of the spark plasma-sintered In₄Se₃-In₄Te₃ material system. Samples of pure In₄Se₃ and In₄Se₃ (80 wt.%)/In₄Te₃ (20 wt.%) mixture were prepared for comparison, and structural, compositional, and thermoelectric characterizations were carried out. The highest ZT of 0.56 was achieved at 672 K in the mixture sample, and the mixing effect of In₄Se₃ and In₄Te₃ on the thermoelectric properties was evaluated.

(Received May 4, 2010; accepted December 11, 2010;
published online January 5, 2011)

EXPERIMENTAL PROCEDURES

The In, Se, and Te raw materials were melted in evacuated quartz ampoules by an induction furnace to prepare In-Se and In-Te ingots. For *n*-type self-doping, the nominal compositions of the In-Se and In-Te ingots were controlled to be $\text{In}_4\text{Se}_{2.5}$ and $\text{In}_4\text{Te}_{2.8}$, respectively. Two-step annealing of the In-Se ingot at 535°C for 48 h and 430°C for 24 h was carried out to produce a homogeneous In_4Se_3 phase. Thermal annealing for the evolution of the In_4Te_3 phase was performed at 420°C for 48 h with the In-Te ingot. The phases were examined by using an x-ray diffractometer (XRD, D/Max-2500/PC, Rigaku). In_4Se_3 was synthesized in a single phase, while In_4Te_3 contained a small amount (~3%) of an In_2Te_5 phase. The annealed In_4Se_3 and In_4Te_3 ingots were pulverized into powders (8 μm to 30 μm). Sintered bodies of In_4Se_3 and the mixture of In_4Se_3 (80 wt.%) and In_4Te_3 (20 wt.%) were prepared by spark plasma sintering under a uniaxial pressure of 70 MPa at 390°C for 5 min (SPS-515S, Sumitomo Coal Mining Co.). The densities of the sintered bodies were measured by the Archimedes method, and the results showed that the relative densities of In_4Se_3 and the mixture were 100% and 97%, respectively. The compositions of the sintered bodies were characterized by electron probe microanalysis (EPMA, JXA-8100, JEOL). Scanning electron microscopy (SEM) was also performed using the JXA-8100 EPMA. The Seebeck coefficient and electrical conductivity were measured by a four-probe method using a thermoelectric measurement system (RZ-2001i, Ozawa Science). The thermal conductivity was measured by a laser flash method (LFA-457, NETZSCH).

RESULTS AND DISCUSSION

Figure 1 shows powder XRD patterns of the spark plasma-sintered In_4Se_3 and In_4Se_3 (80 wt.%)/ In_4Te_3 (20 wt.%) mixture. The sharp diffraction pattern of the pure In_4Se_3 sample indicates that spark plasma sintering is an effective process to produce a sintered body without introducing any secondary phases.² However, the intensity of In_4Se_3 was drastically weakened in the mixture sample. Therefore, it could be proposed that the existence of an In_4Te_3 phase increases the structural instability of the In_4Se_3 phase in the mixture sample during the sintering process. Meanwhile, the peaks of In_4Te_3 were not observed in the diffraction pattern of the mixture sample, but an In_2Te_3 (015) peak was found between the In_4Se_3 (330) and (311) peaks, indicating that a phase transformation of In_4Te_3 to In_2Te_3 occurred during the sintering process.

In this figure, a metallic In phase was also detected in all samples. Although this was not intended, it could be helpful to investigate the exact peak positions of the In_4Se_3 phase by using the diffraction peak of In (101) as a reference. Because the sintering process was performed at 390°C under

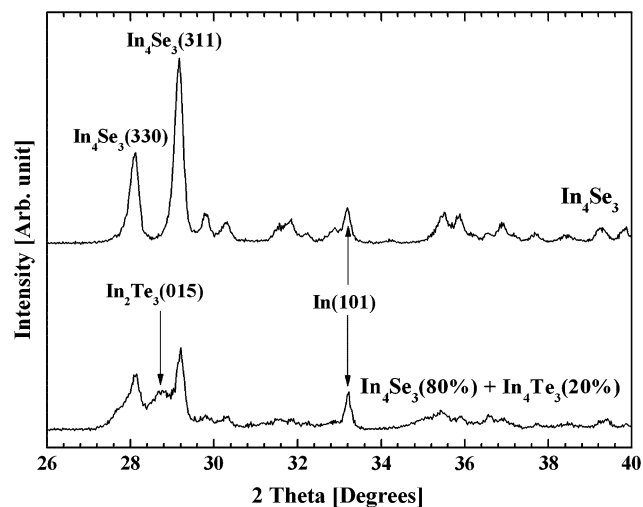


Fig. 1. Powder XRD patterns of spark plasma-sintered In_4Se_3 and In_4Se_3 (80 wt. %)/ In_4Te_3 (20 wt. %) mixture samples.

a pressure of 70 MPa, intermixing of Se and Te atoms is quite plausible in the mixture sample. However, there were no significant differences in the peak positions of In_4Se_3 in the pure and mixture samples.²

Figure 2a shows a SEM micrograph of the pure In_4Se_3 sample, and Fig. 2b and c show EPMA mapping images of In and Se, respectively. Numerous small inclusions were observed in Fig. 2a, and the mapping images in Fig. 2b and c confirmed that they precipitated in the sintered body of In_4Se_3 . Because the nominal composition of this sample was $\text{In}_4\text{Se}_{2.5}$ for the self-doping effect, the excess In could be precipitated. Moreover, In precipitation has been reported even in stoichiometric In_4Se_3 .^{11,12} In the literature, it has been reported that precipitation of In nanoparticles is a result of the decrease in the maximum solubility at the defective region of stoichiometric In_4Se_3 and that the concentration of the In nanoparticles decreases while their average size slightly increases during the thermal annealing process.¹¹ Therefore, the observed In phases in Figs. 1 and 2 could also originate from In nanoparticles merged during the sintering process.

The structure of the In_4Se_3 (80 wt. %)/ In_4Te_3 (20 wt. %) mixture was also investigated by using SEM and EPMA, and the results are shown in Fig. 3. The SEM micrograph in Fig. 3a shows regions in the mixture sample that are distinguishable by their contrast, and the corresponding EPMA mapping images in Fig. 3b–d indicate that the distinctive regions could be categorized by their elemental distributions. Region A, which is composed of only In and Se, could be regarded as the In_4Se_3 phase. Because no Te was found in region A, there was no diffusion of Te from In_4Te_3 to the In_4Se_3 phase during the spark plasma sintering process.

In the B and C regions, all three elements in the mixture sample, In, Te, and Se, were found. The

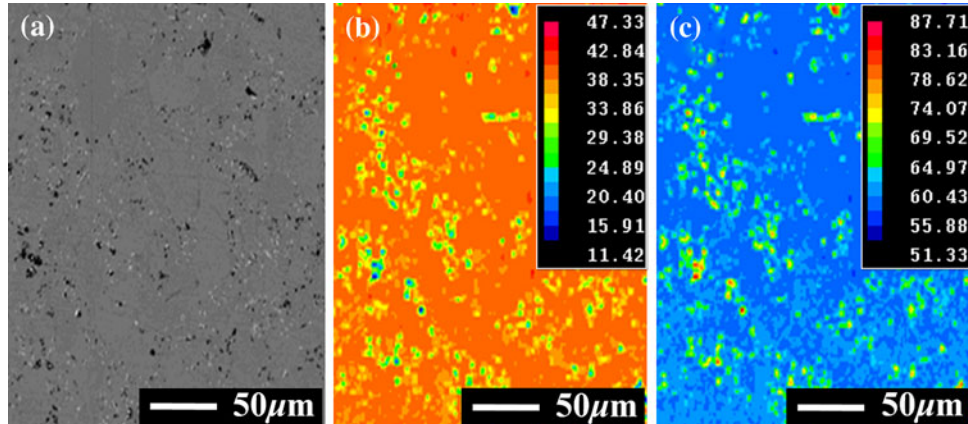


Fig. 2. (a) SEM micrograph of spark plasma-sintered In_4Se_3 and corresponding EPMA mapping images of (b) Se and (c) In. The insets indicate the atomic percentages of the elements.

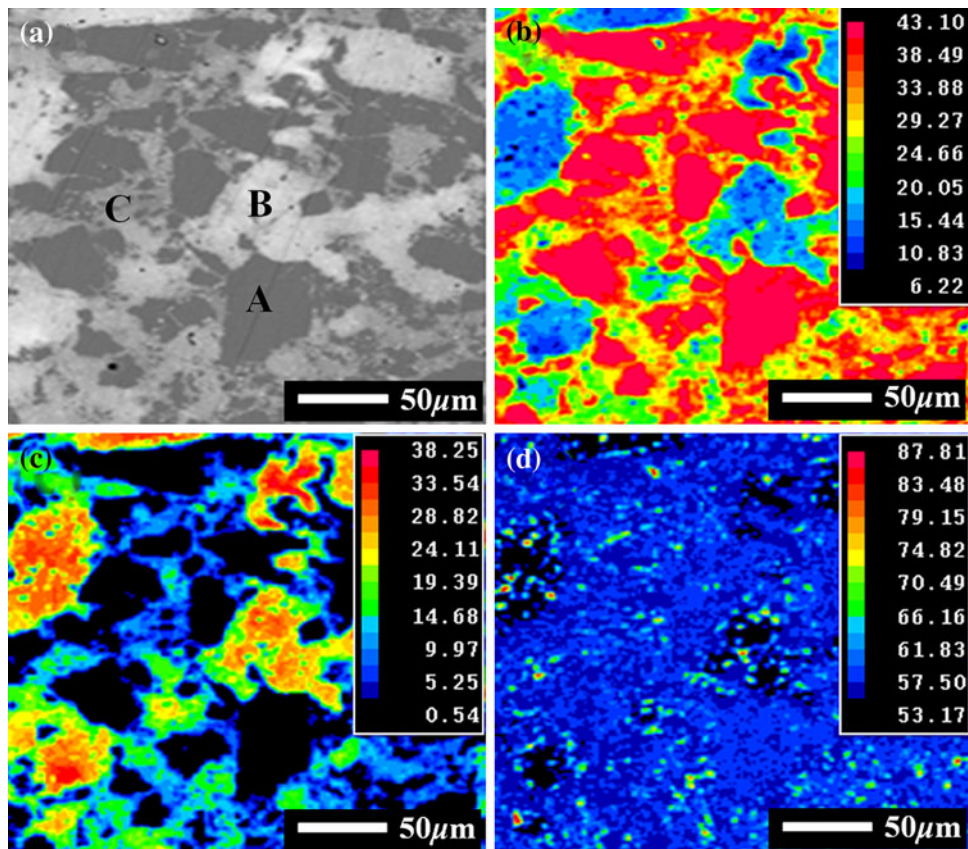


Fig. 3. (a) SEM micrograph of spark plasma-sintered In_4Se_3 (80 wt.%) / In_4Te_3 (20 wt.%) mixture and corresponding EPMA mapping images of (b) Se, (c) Te, and (d) In. The insets indicate the atomic percentages of the elements.

main differences between the B and C regions were the grain size and the fractions of Se and Te in the In-Se-Te phase. Te was more abundant than Se in the B region, where the grain size was relatively large. In the C region, small grains with high Se and Te concentrations were found. This result shows that the In-Se-Te phase in the B and C regions is formed by diffusion of Se from In_4Se_3 to In_4Te_3 . Because the atomic number of Te is larger than that

of Se and the lattice constant of In_4Te_3 is larger than that of In_4Se_3 , preferential diffusion of Se to In_4Te_3 is quite reasonable.¹⁰

Preferential diffusion of Se could lead to deficiency of Se in the In_4Se_3 lattices, resulting in a deterioration of crystallinity, as shown in Fig. 1. However, the lattice parameters of In_4Se_3 did not change significantly due to the Se deficiency, consistent with the result reported by Rhyee et al.² The

In_4Te_3 phase could also be affected by the preferential diffusion. In Fig. 1, only an In_2Te_3 phase was observed and no diffraction peak of the In_4Te_3 phase could be observed, in spite of its significant content of 20% in the mixture sample. Therefore, the In-Se-Te phase in the B and C regions is regarded as a $\text{In}_2(\text{Te}_x\text{Se}_{1-x})_3$ phase, and the Se content in the phase in the C region (small grains) is higher than that in the B region (large grains) due to the more effective diffusion of Se into the small grains. The transformation of the In_4Te_3 phase to the In_2Te_3 phase was accompanied by In precipitation. As shown in Fig. 3d, precipitated In particles were intensively observed in the B and C regions instead of the A region. Therefore, it is proposed that the In_4Te_3 was dissolved into $2\text{In} + \text{In}_2\text{Te}_3$ during the sintering process and that this process could be accelerated by the preferential diffusion of Se.

Figure 4 shows the electrical conductivities, Seebeck coefficients, and power factors of the pure and mixture samples. As shown in Fig. 4a, the pure In_4Se_3 sample had a higher electrical conductivity than the mixture sample at relatively low temperatures. Above 450 K, the conductivities of the pure and mixture samples became nearly identical. From the exponential increase of the electrical conductivity with increasing temperature, it was found that both samples demonstrated semiconducting properties. Below 450 K, the electrical conductivities were higher than the values expected from the exponential increase of the conductivity. Because the temperature of 450 K is slightly higher than the melting temperature of In (~ 430 K), the transition of the electrical conductivity at this temperature may be related to the melting of the precipitated In.³ Therefore, the metallic In precipitation shown in Figs. 1 and 2 may be the origin of this transition behavior.

The electrical conductivity is dependent on the carrier concentration and mobility, which are affected by grain size and boundary properties. In this study, the activation energy of the Arrhenius plot in Fig. 1a was 0.2 ± 0.02 eV in both samples at temperatures above 450 K, which is almost the same value as the direct band gap (0.2 eV) of In_4Se_3 .² Therefore, this implies that thermally excited charge carriers in the In_4Se_3 phase may play an important role in the increased electrical conductivity of both samples at high temperatures.

The Seebeck coefficients of the pure and mixture samples were negative, so they were *n*-type thermoelectric semiconductors. The temperature dependence of the absolute Seebeck coefficient is shown in Fig. 4b. The Seebeck coefficient of the pure sample increased with temperature. However, there was no temperature dependence observed for the mixture sample. The Seebeck coefficient of the mixture sample was in the range of $-250 \mu\text{V/K}$ to $-290 \mu\text{V/K}$. In the literature, it was reported that the Seebeck coefficient of In_4Se_3 decreases with increasing Se deficiency.² In this experiment, the In_4Se_3 phase in the mixture sample had a smaller

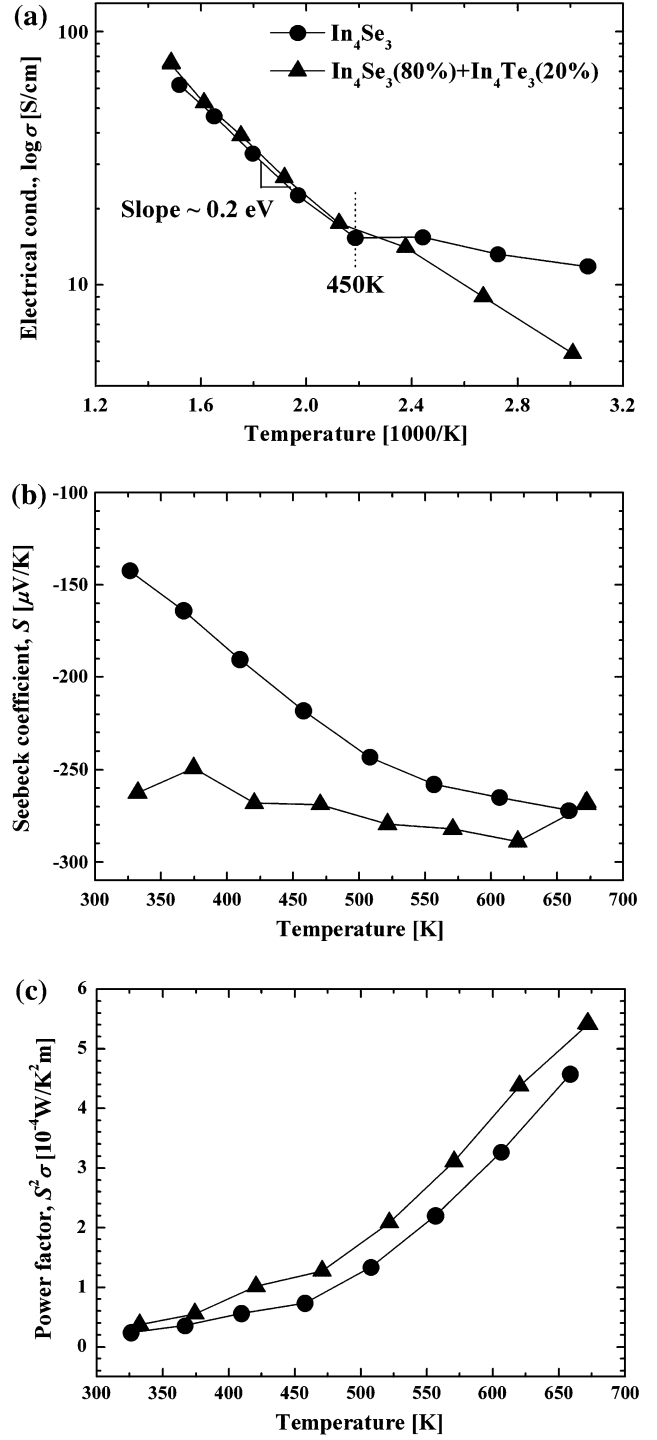


Fig. 4. (a) Arrhenius plot of the electrical conductivity. (b) The Seebeck coefficients and (c) power factors of the pure In_4Se_3 and mixture samples.

amount of Se than pure In_4Se_3 due to the preferential diffusion of Se, as shown in Fig. 3. Therefore, the increase of the Seebeck coefficient in the mixture may originate from the existence of the In_2Te_3 phase. Eventually, the mixture sample shows a higher power factor than the pure In_4Se_3 sample, as shown in Fig. 4c.

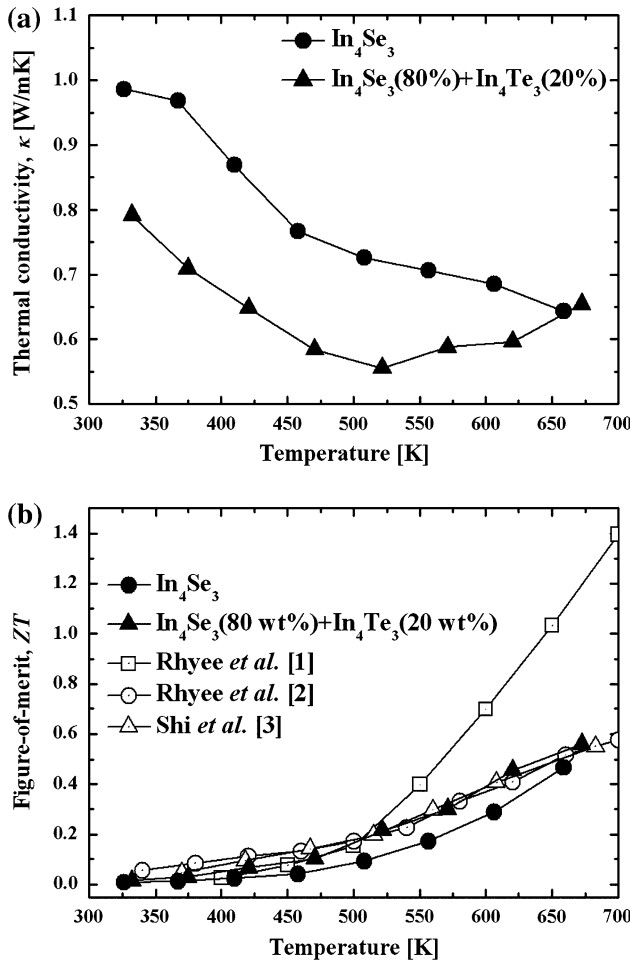


Fig. 5. Temperature dependence of (a) the thermal conductivity and (b) the dimensionless figure of merit of the pure In_4Se_3 and mixture samples.

Figure 5 shows the thermal conductivity and dimensionless figure of merit (ZT) of the pure and mixture samples. The thermal conductivity of the pure sample monotonically decreased with increasing temperature from 0.97 W/mK to 0.64 W/mK, and is quite similar to that reported in Ref. 2. The origin of such a low thermal conductivity could be Peierls distortion, the condensate state, and the abundance of low-frequency phonon modes in the In_4Se_3 structure.^{1,6,7,13} In the mixture sample, the thermal conductivity was much lower, and the lowest value of 0.56 W/mK was obtained at 520 K. This indicates that the irregularity of the lattice in the mixture sample could retard the thermal transport even more. Consequently, the highest ZT of 0.56 at 672 K was obtained in the mixture sample, as shown in Fig. 5b. Although this result is quite similar to the values in Refs. 2 and 3, it was proven that the mixing of In_4Se_3 and In_4Te_3 is effective to enhance the thermoelectric properties in our material systems. The ZT of Ref. 1 was obtained from a directionally grown In_4Se_3 sample prepared by the Bridgeman

method, and its high electrical conductivity is regarded as the main origin of the high ZT .

As shown above, improved thermoelectric properties were demonstrated in the In_4Se_3 (80 wt%)/ In_4Te_3 (20 wt%) mixture sample compared with pure In_4Se_3 . In this sample, the increased Seebeck coefficient and lower thermal conductivity could be achieved without a loss of electrical conductivity. This result can provide future possibilities for engineering thermoelectric In_4Se_3 -based material systems by alloying or doping.

CONCLUSIONS

We investigated the structural and thermoelectric properties of spark plasma-sintered In_4Se_3 and In_4Se_3 (80 wt%)/ In_4Te_3 (20 wt%) mixture samples. In contrast to pure In_4Se_3 , a phase transformation from In_4Te_3 to In_2Te_3 was observed in the mixture sample after the sintering process. Because of the differences in atomic number between Se and Te and in the lattice parameters between In_4Se_3 and In_4Te_3 , preferential diffusion of Se from In_4Se_3 to In_4Te_3 was clearly observed in the mixture sample, the effect of which on the structural properties was revealed. The highest ZT of 0.56 at 672 K was achieved in the mixture sample, and the mixing effect of In_4Se_3 and In_4Te_3 on the thermoelectric properties was evaluated.

ACKNOWLEDGEMENTS

This research was supported by a Grant from the Fundamental R&D Program for Core Technology of Materials funded by the Ministry of Knowledge Economy, Republic of Korea.

REFERENCES

1. J.-S. Rhyee, K.H. Lee, S.M. Lee, E. Cho, S.I. Kim, E. Lee, Y.S. Kwon, J.H. Shim, and G. Kotliar, *Nature* 459, 965 (2009).
2. J.-S. Rhyee, E. Cho, K.H. Lee, S.M. Lee, S.I. Kim, H.-S. Kim, Y.S. Kwon, and S.J. Kim, *Appl. Phys. Lett.* 95, 212106 (2009).
3. X. Shi, J.Y. Cho, J.R. Salvador, J. Yang, and H. Wang, *Appl. Phys. Lett.* 96, 162108 (2010).
4. D.T. Morelli, V. Jovovic, and J.P. Heremans, *Phys. Rev. Lett.* 101, 035901 (2008).
5. B. Wölfling, C. Kloc, J. Teubner, and E. Bucher, *Phys. Rev. Lett.* 86, 4350 (2001).
6. D.M. Bercha, L.Y. Kharkhalis, A.I. Bercha, and M. Sznajder, *Phys. Stat. Sol. (b)* 203, 427 (1997).
7. L.S. Kukushkin, *Zh. Eksp. Teor. Fiz. Pis'ma* 7, 194 (1968).
8. D.M. Bercha and K.Z. Rushchanskii, *Phys. Solid State* 40, 1906 (1998).
9. E.G. Lavut, N.V. Chelovskaya, E.V. Anokhina, V.N. Denim, and V.P. Zlomanov, *J. Chem. Thermodyn.* 27, 1337 (1995).
10. D.M. Bercha and K.Z. Rushchanskii, *Phys. Solid State* 41, 1693 (1999).
11. V.M. Garamus, A.K. Islamov, Y.P. Pilat, and V.P. Savchin, *Phys. Solid State* 40, 223 (1998).
12. J.-C. Tedenac, G.P. Vassilev, B. Daouchi, J. Rachidi, and G. Brun, *Cryst. Res. Technol.* 32, 605 (1997).
13. D.M. Bercha, L.Y. Kharkhalis, A.I. Bercha, and M. Sznajder, *Semiconductors* 31, 1118 (1997).